Annu. Rev. Phys. Chem. 1996. 47:135–69

UNDERSTANDING NMR CHEMICAL SHIFTS

Cynthia J. Jameson
Department of Chemistry M/C-111, University of Illinois at Chicago, Chicago, Illinois 60607-7061

KEY WORDS: nuclear magnetic shielding, rovibrational averaging, intermolecular effects, shielding surface, adsorbed species

ABSTRACT

The NMR chemical shift serves as a paradigm for molecular electronic properties. We consider the factors that determine the general magnitudes of the shifts, the state of the art in theoretical calculations, the nature of the shielding tensor, and the multidimensional shielding surface that describes the variation of the shielding with nuclear positions. We also examine the nature of the intermolecular shielding surface as a general example of a supermolecule property surface. The observed chemical shift in the zero-pressure limit is determined not only by the value of the shielding at the equilibrium geometry, but the dynamic average over the multidimensional shielding surface during rotation and vibration of the molecule. In the gas, solution, or adsorbed phase it is an average of the intermolecular shielding surface over all the configurations of the molecule with its neighbors. The temperature dependence of the chemical shift in the isolated molecule, the changes upon isotopic substitution, the changes with environment, are well characterized experimentally so that quantum mechanical descriptions of electronic structure and theories related to dynamics averaging of any electronic property can be subjected to stringent test.

INTRODUCTION

Fifty years after its discovery, nuclear magnetic resonance (NMR) spectroscopy is widely used in the identification of molecules and the elucidation of molecular structure and dynamics. NMR can determine average distances between nuclei (such as proton-proton distances in a protein), the numbers of equivalent

0066-426X/96/1101-0135$08.00

and nonequivalent neighbors (from spin-spin coupling information), the types of functional groups in which each NMR nucleus is found (from chemical shift information), and dynamic information spanning seconds to picoseconds. That the nuclear magnetic moment has a resonance frequency shift from one electronic environment to another and that such shifts can be measured in one part per hundred million has made the chemical shift a very good empirical tool in distinguishing differences in electronic environment that arise from chemical reaction, geometric isomerism, hydrogen bonding, adsorption, etc. The use of these observations in an empirical manner is commonplace. There have been such a large number of isotropic chemical shifts measured for protons in various environments that a very large data base is now available and can be used empirically to predict all the proton shifts in a new molecule. The same can be said of carbon shifts, and perhaps other nuclei will in time yield to such predictions based on empirical correlations. Calculations of the NMR chemical shift from first principles has reached the point, in the past few years, of providing quantitative agreement with experiment in some cases, such that both the small effects that have to do with rovibrational averaging and medium effects have to be taken into account when comparing theoretical calculations with experiment. Theoretical calculations must in fact be used hand in hand with experiments in which the tensor quantity is measured rather than the isotropic average observed in a randomly tumbling molecule. The theoretical calculations yield the orientation of the principal axes of the calculated tensor and provide the link between the measured individual components of the tensor and the molecular framework.

In this review we consider the NMR chemical shift as a molecular electronic property not unlike the electric dipole polarizability, for example. We consider the factors that determine the general magnitudes of the shifts, the state of the art in theoretical calculations, the nature of the shielding tensor, and the molecular electronic property surface in terms of geometry modifications as they occur in vibration and torsion. We also consider the nature of the intermolecular shielding surface as a general example of a supermolecule property surface.

The multidimensional shielding surface that describes the variation of the shielding with nuclear positions is analogous to the potential energy multidimensional surface. From the dependence of the nuclear shielding on the configuration of the nuclei (the distances and the bond angles between them), it is possible to calculate observed quantities such as the temperature dependence of the chemical shift of a nucleus in a molecule in a gas in the zero-pressure limit and the dependence of the chemical shift on the isotopic masses of the atoms in the immediate vicinity of the NMR nucleus. What determines the observed shielding in the limit of independent molecule is not only the value

on this shielding surface at the minimum energy (equilibrium) geometry, but also the averaging over this surface during the rotation and vibrations of the molecule. For molecules in a gas, solution, or adsorbed fluid on a heterogeneous surface, the observed chemical shift is averaged not only over all the populated rovibrational states, torsions, and librations, but also over all the ensembles of the molecule with its neighbors.

No other molecular electronic property has been characterized as well as the NMR chemical shift in terms of its virial coefficients, mass dependence, and temperature dependence. The ultra high resolution afforded by the NMR measurement, combined with the exquisite sensitivity of the shielding, makes it possible to characterize this molecular property in detail experimentally. The change of the electric dipole polarizability with internuclear separation in a rare gas pair, for example, is one of the pair interaction properties that serve very well as tests of theories and physical models but are very difficult to measure. Contrast this with the well-characterized ^{129}Xe shielding as a function of density and temperature in the dilute gas. The dependence of few other property surfaces on intramolecular nuclear coordinates has been extensively explored. The experimental observations of the temperature dependence in the rotating-vibrating isolated molecule and the changes upon substitution of a remote atom by a heavier isotope are well characterized in the chemical shift, unlike in any other molecular electronic property. The theories associated with the rovibrational averaging of any electronic property can be tested for shielding, where both experiments and theoretical calculations are feasible. In other words, the NMR shielding serves as a paradigm for the exploration of the dependence of a molecular electronic property on intramolecular coordinates and masses, as well as on intermolecular separations, temperature, electric fields, field gradients, and grand ensemble configurations.

GLOBAL TRENDS ACROSS THE PERIODIC TABLE

A measurement in the laboratory provides a chemical shift δ between the sample and the reference substance, i.e. a difference in the nuclear magnetic shieldings such as

$$\delta = \sigma(\text{nucleus } {}^{\mu}\text{A, in molecule } {}^{\mu}\text{AXY, in solvent AB, } x_{AXY}, x_{AB}, T)$$
$$- \sigma(\text{nucleus } {}^{\mu}\text{A, in molecule } {}^{\mu}\text{AB, in solution with AXY, } x_{AXY}, x_{AB,} T).$$

It turns out that it is important to specify completely all the variables (e.g. mole fractions x_{AB}) that determine the observed chemical shift, because the nuclear magnetic shielding is so sensitive to factors of molecular structure and environment. How sensitive a nucleus is to molecular structure and environment

varies a great deal from one nucleus to another across the periodic table. The chemical shift range—the chemical shift between the least-shielded and the most-shielded nucleus of an element—depends on the position of the element in the periodic table. The sum-over-states perturbation expression derived by Ramsey for the nuclear magnetic shielding (1),

$$\sigma_{\alpha\beta} = \sigma^{\mathrm{d}}_{\alpha\beta} + \sigma^{\mathrm{p}}_{\alpha\beta},$$

where the diamagnetic and paramagnetic terms are

$$\sigma^{\mathrm{d}}_{\alpha\beta} = (\mu_0 \mathrm{e}^2/8\pi\,\mathrm{m})\left\langle 0 \middle| \sum_{\mathrm{k}} \{(r^2\delta_{\alpha\beta} - r_{\mathrm{k}\alpha} r_{\mathrm{k}\beta})\}/\mathrm{r}_{\mathrm{k}}^3 \middle| 0 \right\rangle$$

and

$$\sigma^{\mathrm{p}}_{\alpha\beta} = (\mu_0 \mathrm{e}^2/8\pi\,\mathrm{m}^2) \sum_{n}{}' (\mathrm{E}_n - \mathrm{E}_0)^{-1} \times \left[\left\langle 0 \middle| \sum_{\mathrm{k}} \ell_{\mathrm{k}\alpha}/{r_{\mathrm{k}}}^3 \middle| n \right\rangle \cdot \left\langle n \middle| \sum_{\mathrm{k}} \ell_{\mathrm{k}\beta} \middle| 0 \right\rangle + \mathrm{c.c.} \right]$$

highlights the important factors. Jameson & Gutowsky (2) predicted that the sensitivity of the chemical shifts to changes in the chemical environment would scale according to the characteristic $\langle a_0^3/r^3 \rangle$, which is obtained from the spin-orbit splittings in atomic spectra, for the valence p shell (or d for transition elements) of the free atom in its ground state. This is clearly demonstrated by the correlation with this quantity of the ranges of the chemical shifts of the nuclei observed in periodic table–wide trends (3). Approximately 20 years later, this fundamental atomic quantity also provides a reasonable estimate of the relative magnitudes of chemical shifts in analogous compounds. The chemical shifts in one set of compounds (e.g. containing ^{125}Te) plotted against those of the analogues (containing ^{77}Se) have a slope of the order of the ratio of the $\langle a_0^3/r^3 \rangle$ for Te and Se atoms. The presence of low-lying electronic states connected to the ground state by magnetic dipole transitions enhances the range of chemical shifts of transition metal nuclei, and symmetry dictates which matrix elements have significant contributions to the paramagnetic term, e.g. for nuclei in linear molecules, only the perpendicular component of the tensor does not vanish.

THEORETICAL CALCULATIONS OF NUCLEAR MAGNETIC SHIELDING

The terms in the total energy of a molecule that are bilinear in the external homogeneous magnetic field and the nuclear magnetic moment determine the

nuclear magnetic shielding for a nucleus in a molecule. Using the sum-over-states form of the Ramsey equations in an uncoupled approach usually leads to rather poor ab initio results because the interelectron interactions have not been calculated in the presence of the perturbing magnetic field. A general approach to calculations of second-order molecular electronic properties, the coupled Hartree-Fock (CHF) method, can be systematically improved by extending the basis set size (4).

The magnetic field B does not appear directly in the electronic Hamiltonian; rather it is represented by the magnetic vector potential that is related to B according to $B = \nabla \times A$. The formalisms for calculations of magnetic properties (as in the Ramsey expressions) usually employ the Coulomb gauge for the definition of the magnetic vector potential: $A(\mathbf{r}) = (1/2)\mathbf{B} \times \mathbf{r}$. Other choices are possible (5). Because the magnetic vector potential is not unique (any gauge transformation, such as a translation of the origin, leads to a new vector potential for the same magnetic field), the separation between the diamagnetic and paramagnetic parts is not unique. Although the sum (of the so-called diamagnetic and paramagnetic terms, as expressed by Ramsey) is gauge invariant when the calculations are done in a complete basis set, in actual calculations the basis set is incomplete, and in principle any result may be obtained with the same basis set by using various gauge origins. This arises because the quality of the calculation of the diamagnetic part (as expressed by Ramsey, in terms of only the ground electronic state function) is not balanced by the quality of the calculations of the paramagnetic shielding, which involves excited state wavefunctions. In the conventional CHF approach, one chooses a gauge origin for the magnetic vector potential and uses large basis sets, extending the size of the basis until the results are reasonably independent of the chosen gauge origin (6, 7a,b).

The shielding calculation can also be based on analytic derivatives; the shielding is the second derivative of the molecular energy with respect to the simultaneous perturbation of the nuclear magnetic moment and the external magnetic field (8). Geertsen (9, 10) has shown that the diamagnetic part can be expressed in the same formalism as the paramagnetic part, i.e. in terms of the excited state functions, but this still requires that the calculations be carried out with very large basis sets.

The advances in the past ten years have involved methods of getting around the gauge problem. One way to resolve the difficulty is to use basis functions that explicitly depend on the external homogeneous magnetic field with the same factor that would be found for the correct first-order wavefunction for a central field problem in a magnetic field. The basis set of gauge including atomic orbitals (GIAOs), or London orbitals, has been used by Ditchfield (11),

and more recently, Pulay and coworkers (12) employed it in efficient shielding calculations within an analytic gradient formalism. GIAOs constitute a physically motivated, compact basis set for magnetic calculations. They represent to first order the eigenfunctions of a one-electron system that has been perturbed by an external magnetic field. The field-dependent exponential factor in the London orbital depends on the origin of the coordinate system. A displacement of the origin changes the phase factor of an orbital centered on a nucleus by a factor that is independent of the electronic coordinates. Thus, the calculated properties such as shielding or magnetic susceptibility remain unaffected, and methods based on the use of such orbitals are gauge invariant at any basis set size. That gauge factors are attached to molecular orbitals characterizes the individual gauge for localized orbitals (IGLO) method introduced by Schindler and Kutzelnigg (13, 14). The localized orbital–local origin (LORG) method introduced by Hansen & Bouman (15) and the IGLO method rely on using identities and closure relations that are only approximately valid for finite basis sets, and the expressions used in both methods reduce to the same form in the limit of a complete basis set (16).

Another method for calculation of nuclear shieldings and magnetizabilities, individual gauges for atoms in molecules (IGAIM), uses the calculation of molecular current density distributions (17). The IGAIM approach amounts to constructing the induced current density distribution of a molecule from its constituent atoms. The induced first-order current density is determined accurately over each spatially defined atom in a molecule by using its nucleus as origin in a set of separate conventional CHF calculations.

All these methods minimize or eliminate the gauge dependence of the result, compared to the conventional (common origin) CHF method, by using distributed gauge origins in some form or another. Medium-sized basis sets (triple zeta with two or more polarization functions) when used with any one of these distributed gauge origin approaches (GIAO, IGLO, LORG, or IGAIM) can successfully provide isotropic shieldings and shielding tensors for nuclei in the first and second row of the periodic table (see for example the quality of agreement between calculated and experimental shielding tensor components in Figure 1) but not in certain "pathological" molecules such as CO, N_2, HCN, F_2, and NNO. These methods have all been extended to include electron correlation by multiconfiguration self-consistent field (MCSCF) (18, 19), by Müller-Plesset perturbation expansion (20), or by second-order propagation theory (21, 22).

For the pathological molecules, higher-order contributions in many-body perturbation theory (MBPT) need to be taken into account. MBPT (2) frequently overestimates the correlation corrections to the shielding. This overestimation of electron correlation contributions is reduced at the third- and partial-fourth order MBPT (20). Gauss has developed higher-level shielding theory based

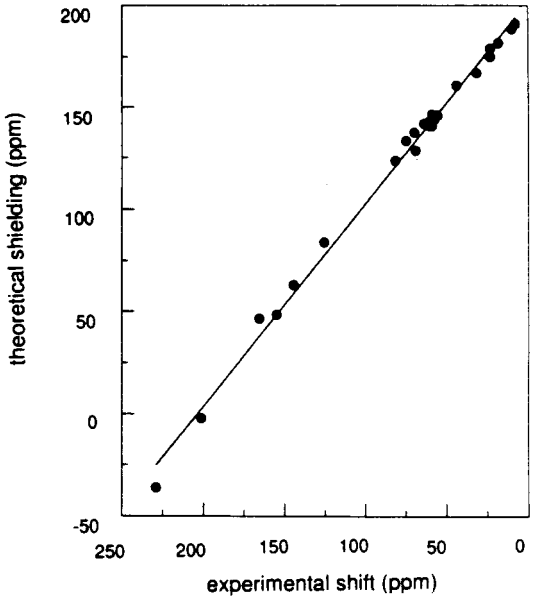

Figure 1 Comparison of calculated ^{13}C shielding tensor components for all seven carbons in the amino acid threonine with experimental values in the single crystal. (Reproduced from Reference 104, with permission.)

on the GIAO ansatz for calculations at the coupled cluster singles and doubles, with an approximation for triplet excitations (20). In a systematic study of a set of pathological molecules, Gauss (20) has shown that higher-level treatment provides superior predictions of absolute shielding constants, while relative shifts are less sensitive to higher-order correlation effects. For reproducing relative shifts, a higher-level treatment is warranted only when second-order MBPT and SCF results differ appreciably (23).

Density functional methods are being devised for calculations of magnetic properties (24–28). At present the applications to shieldings do not yet correctly include the current density dependence in the exchange-correlation functionals (29a,b, 30). Nevertheless, shielding calculations using density functional theory have had reasonable success, especially for systems such as O_3 in which correlation plays an important role in shielding. A magnetic field density functional theory has been proposed that would involve the use of only the zero-field electron density in the calculations of nuclear shielding (31, 32), but a good approximation to the magnetic field functional has not yet been constructed. For a recent review of the theoretical methods, see Chesnut (33), and for a yearly update of the theoretical and physical aspects of nuclear shielding, see Jameson in the series *Nuclear Magnetic Resonance* (34).

THE CONNECTION BETWEEN CHEMICAL SHIFTS AND MOLECULAR STRUCTURE

The proceedings of a workshop on the recent advances in the connection between chemical shifts and molecular structure provide a useful overview (35). The chemical shift of a nucleus identifies the functional group in which the nucleus is sited. This itself provides clear structural information. More detailed structural information—such as axial versus equatorial, syn versus anti, hydrogen-bonded or not—also come easily. No wonder that NMR is widely used for proof of structure of new compounds. A demonstration of the power of the chemical shift-to-structure connection is provided by the inequivalencies of ^{13}C chemical shifts in the various alanines, for example, in a protein. Oldfield et al (36–38) have mapped the ^{13}C shielding as a function of the torsion angles π and ψ in peptide models. These theoretical shielding surfaces have been found to be sufficient in explaining ^{13}C chemical shifts in proteins (38). The secondary structure of the protein causes the local structure of the C^{α}, for example, of the alanines to differ, and the unique set of π and ψ torsion angles for each local structure leads to different chemical shifts (39).

The Shielding Tensor as an Index of Electronic Structure

Theoretical calculations of nuclear magnetic shielding provide the entire shielding tensor on an absolute basis, that is, with respect to a bare nucleus. On the other hand, a measurement in the laboratory provides a chemical shift δ between the sample and the reference substance, that is, a difference in shielding such as

$$\delta_{xx} = \sigma_{\text{iso}}\left(^{13}\text{C in SiMe}_4\text{, liquid, 300 K}\right) - \sigma_{xx}\left(^{13}\text{C in CS}_2\text{, Ar martix, 21 K}\right).$$

Changes in shielding occur when moving from the isolated molecule in its rigid equilibrium geometry to the single molecule in its ground vibrational state at 0 K, to the molecule in the gas at the zero-pressure limit at 300 K, to the molecule in a solution or a single crystal or an Ar matrix or powder. These changes are not necessarily small and are not the same for the sample and the reference substance. Therefore, accurate comparisons between theoretically calculated values of the absolute shielding tensor and the published chemical shift data cannot be made without taking into account the intramolecular vibrational averaging and the intermolecular effects on the shielding. Furthermore, it is useful to have experimental absolute shielding values rather than chemical shifts to compare with when evaluating theoretical calculations. The absolute shielding scale is set via the identity that relates shielding and spin rotation tensors. A

measured spin-rotation tensor for the nucleus in a primary standard molecule (e.g. ^{13}C in CO molecule, ^{19}F in HF, ^{31}P in PH_3, ^{17}O in CO, ^{15}N in NH_3, ^{29}Si in SiH_4) in the gas phase in the limit of zero pressure or in a molecular beam defines the absolute shielding for the standard. The measured chemical shift between molecule A and the primary standard molecule in the same sample in the gas phase then provides the absolute isotropic shielding value for the nucleus in any molecule A. In principle, only one point on the scale need be established, and this permits all measured chemical shift differences for that nucleus to be converted to absolute shielding (i.e. relative to the bare nucleus).

From the early days ($\sim$50 years ago) of chemists' involvement in NMR spectroscopy, the NMR chemical shift has been the primary NMR structure parameter as a result of its intimate connection with the molecular electronic structure and its exquisite sensitivity to changes in chemical environment. Only in the past few years have the theoretical calculations been sufficiently accurate to predict chemical shift variations on the order of 5 ppm in ^{13}C chemical shifts in reasonably large molecules such as sugars. Thus, our basic understanding of the NMR chemical shift or nuclear magnetic shielding is now beginning to provide an adequate foundation for interpreting shift values in more than an empirical way. At the same time, a sufficient body of experimental data on chemical shift tensors upon which structural correlations can be based has become available. It is the availability of chemical shift tensor data that has driven the improvements in the shielding computations, because the tensor quantity with six parameters per nucleus provides considerably more information for characterizing the three-dimensional electronic structure of molecules. The six parameters at a nuclear site are usually expressed as three principal values in a principal axes frame plus three orientational parameters relating this frame to the crystalline axes, for example, or to the inertial axes of the molecule.

The ^{13}C shift tensors in small organic molecules dispersed in a solid Ar matrix at 20 K provide a rich source of information (40–42). The assignment of the experimental tensor components has been aided by ab initio theoretical computations of the shielding tensor, especially in cases where the nuclear site symmetry alone does not lead to unequivocal assignments. Tensor information for a family of molecules provides structure-tensor correlations, the interpretation of which provides the basis of our understanding of this very sensitive index of a nuclear site in a molecule in an environment. For example, in an aromatic system such as pyrene (4 benzene rings fused together), there are 5 unique nuclear sites among the 16 carbons (43). One of the principal axis directions at each ^{13}C site is, by symmetry, perpendicular to the plane of the molecule. Along this direction lies the highest shielding component of each of the ^{13}C tensors, without exception. The large positive shielding component

perpendicular to the molecular plane is a general characteristic of planar aromatic molecules. General trends in the least-shielded (highest frequency) component σ_{11} are observed: σ_{11} tends to lie along the bond with the smallest bond order or perpendicular to the bond of largest bond order. When two of the three bond orders are equal, σ_{11} lies along the unique bond when its bond order is the smallest or perpendicular to the unique bond when its bond order is the largest. In the case where all three bonds exhibit different bond orders, the σ_{11} axis strikes a compromise between being parallel to the bond with the lowest bond order and perpendicular to the bond with the highest bond order. These observations, based on the single crystal study of pyrene, hold for the entire class of planar aromatic molecules. Thus, the shielding tensor is a sensitive index of the bonding situation around the carbon nuclear site (44). In a dramatic application of ab initio calculations toward the elucidation of the shielding tensor and its dependence on molecular geometry, it has been shown that the departures from D_{2h} symmetry observed in the experimental chemical shift tensor components of naphthalene in the single crystal (leading to the reduced symmetry, C_i) could be accounted for entirely by small geometrical variations that are smaller than the error bars of the X-ray diffraction parameters (45). This leads to the conclusion that solid state NMR methods can be used for refining structural data, especially in those cases in which imperfections such as translational disorder or occlusion of molecular impurities degrade diffraction data but have no effect on chemical shift data.

The shielding tensors associated with the amide fragment in peptides are of great interest because of their potential in the determination of protein secondary structure, conformation, and intramolecular hydrogen bonding. For example, the ^{15}N chemical shift tensors for the peptide nitrogen in alanine residues in polypeptides in various conformations are distinct from each other; σ_{11} and σ_{22} are smaller (less shielded) for the β-sheet compared to the α-helix. The principal axes of the nitrogen shielding tensor vary somewhat, depending on the peptide. Measured chemical shift tensors are compiled in Reference 46.

THE SHIELDING SURFACE FOR A NUCLEUS IN A MOLECULE

A shielding surface is a mathematical surface providing the nuclear shielding value (usually the isotropic average over all magnetic field directions, but also an individual tensor component) as a function of the nuclear coordinates of the system. In the case of an isolated molecule, the intramolecular shielding surface is usually expressed in terms of nuclear displacement coordinates, such as curvilinear internal coordinates or the symmetry adapted linear combinations

of these, the symmetry coordinates. In the case of intermolecular shielding surfaces, the internal coordinates of the supermolecule are used, and the shielding is expressed relative to the completely separated interacting molecules, including counterpoise corrections. The first complete shielding surface was calculated for the H_2^+ molecule by Hegstrom (47). This surface showed the nuclear shielding for the separated atoms, all the way to the united atom, which in this case was a He^+ ion. From the large positive united atom value, the shielding decreases until it reaches a minimum, which occurs at an internuclear separation much longer than the equilibrium bond length and proceeds to the limiting value at infinite separation. Prior to this complete surface, however, Stevens and Lipscomb had discovered, through calculations, the behavior of the shielding in diatomic molecules in the immediate vicinity of the equilibrium geometry for LiH, HF, CO, and N_2 (48–51). The derivative of the shielding with bond distance is negative in all cases except for the Li nucleus in LiH. Ditchfield's calculations of shieldings in the vicinity of the equilibrium bond length verified these results for LiH and for HF, and in addition provided similar results for the H_2 molecule (52). Chesnut (53) evaluated first derivatives of the shielding for the first- and second-row hydrides and found similar results for H_2, HF, and HCl. NaH behaved similarly to LiH (53), and the second derivatives in HCl and HF (54) as well as CO, N_2, CN^-, and F_2 (55) were also negative for all nuclei. That is, both nuclei in the diatomic molecule become deshielded as the bond lengthens, with the exception of the Li and the Na nuclei in LiH and NaH. The unusual behavior of the alkali nuclei remained a puzzle until the complete shielding surface of the NaH molecule was calculated by Jameson & de Dios (56). The complete surface for ^{23}Na in NaH molecule looks very similar to the shielding surface for the H_2^+ molecule (see Figure 2). The difference is the relative positions of the minima in the shielding surface and the potential energy surface (56).

For triatomic and larger polyatomic molecules, the shielding surface is of higher dimensionality. The surface is best expressed in the nuclear displacement coordinates of the molecule, such as symmetry coordinates. Examination of the details of the shielding surface is best carried out by displaying traces on the surface corresponding to keeping some of the coordinates constant. This was done for the first time by Raynes and coworkers for the nuclei in the H_2O molecule (57), followed by the nuclei in the CH_4 molecule (58). Jameson and de Dios calculated the shielding surfaces for the N nucleus in NH_3 (59) and P in PH_3 (60). In these calculations the inversion coordinates of both NH_3 and PH_3 were explored over a wide range of values (59, 60). When examined together, these four surfaces have some features in common. The shielding of the non-H nuclei uniformly decreases with an increase in the symmetric stretch coordinate. The asymmetric stretch coordinates and the asymmetric angle deformation

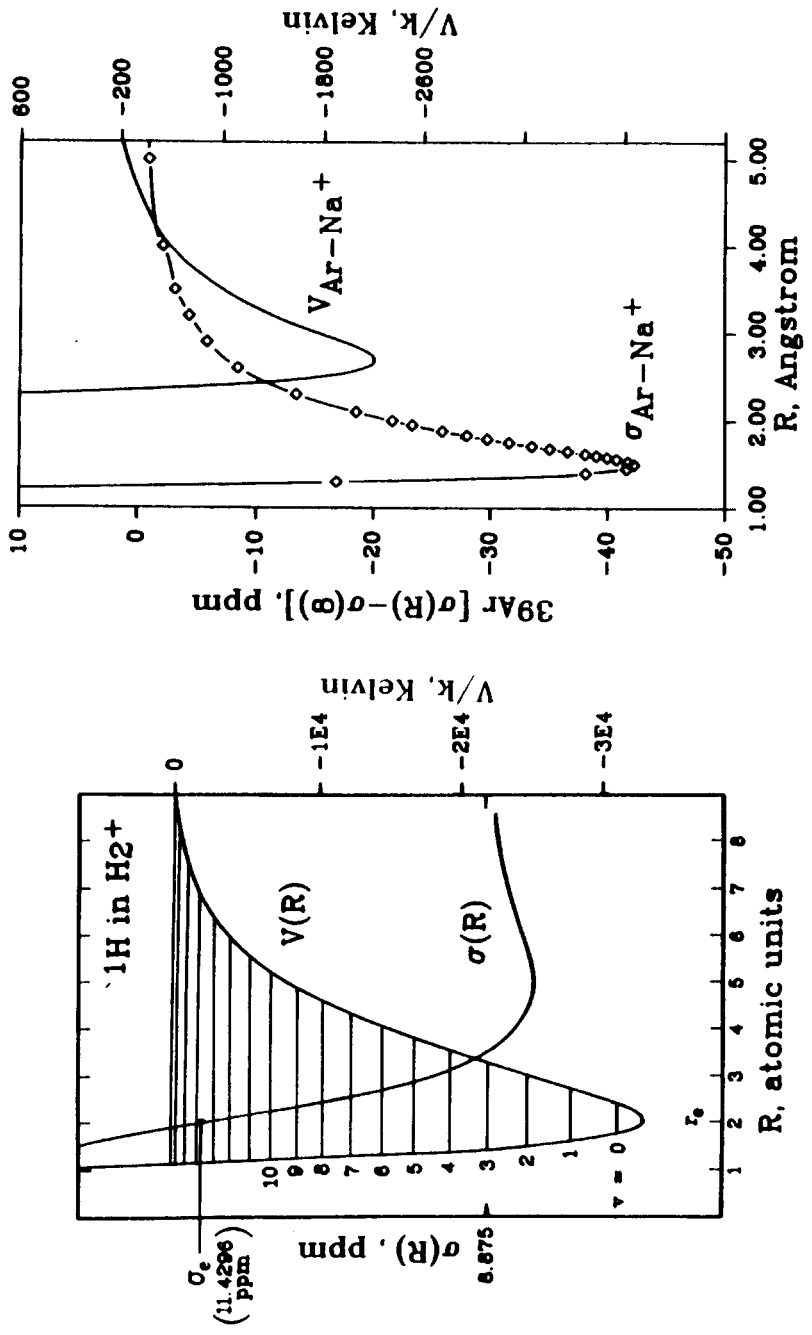

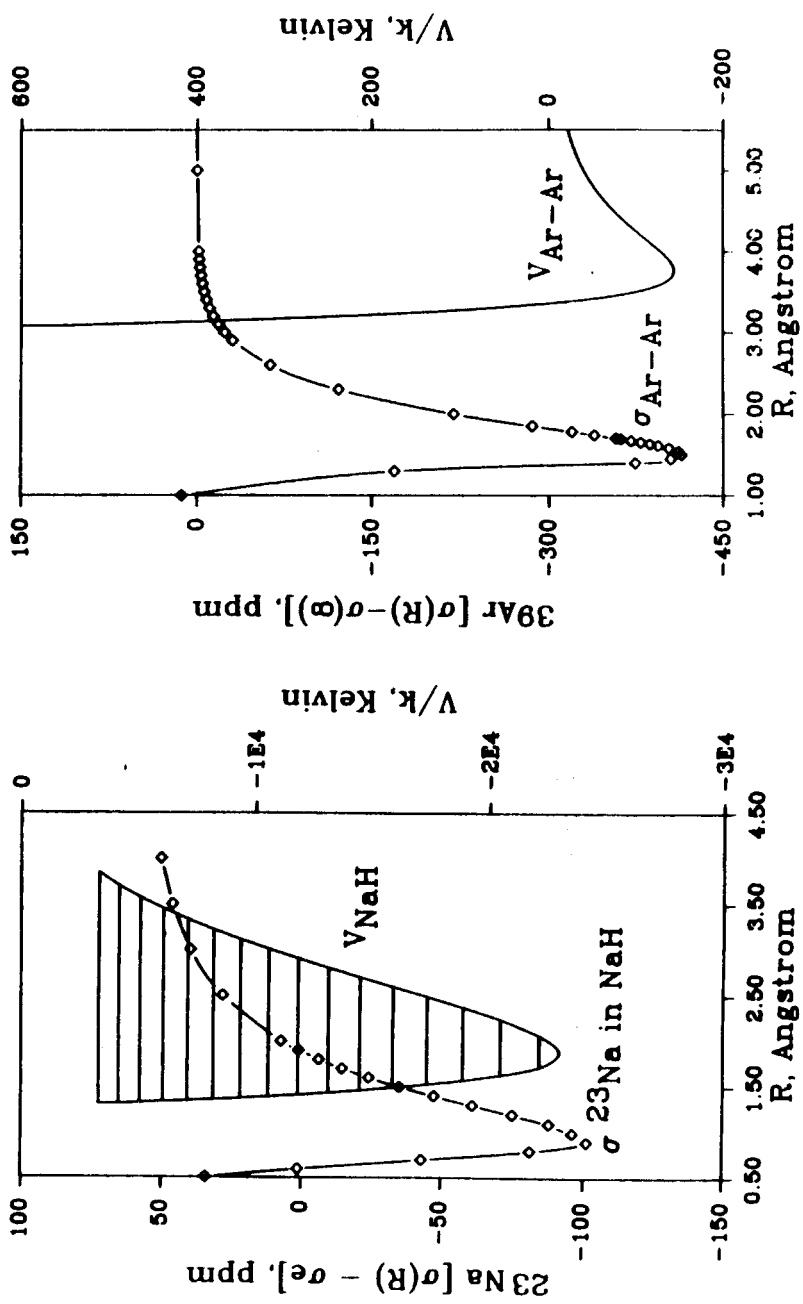

Figure 2 Nuclear shielding surfaces from ab initio calculations and potential energy surfaces for H_2^+, ^{23}Na in NaH, ^{39}Ar in Ar-Na^+ and Ar-Ar. (Reproduced from Reference 56, with permission.)

coordinates have zero first derivatives by symmetry, and therefore these traces are symmetric functions with respect to positive or negative displacements away from the equilibrium coordinates. They are concave in opposite directions. One (the asymmetric stretch) is concave downward (deshielding with increasing displacement from equilibrium), whereas the other (the asymmetric angle bend) is concave upward (increasing shielding with increasing displacement from equilibrium).

The traces on the shielding surfaces corresponding to the opening of the bond angle (the bond lengths being kept constant) in the H_2O, H_2S, H_2Se, NH_3, and PH_3 molecules are concave upward with minimum shielding at the tetrahedral angle (53, 57, 59–61). The equilibrium bond angle for H_2O and NH_3 is very close to tetrahedral, whereas for H_2Se and PH_3 it is less than tetrahedral. H_2Se and PH_3 shielding surfaces have a sizable slope at the equilibrium bond angle.

Other molecules have only been studied in terms of the derivatives of the shielding with respect to bond extension at the equilibrium geometry. The first derivatives of the non-H nuclear shielding in the first- and second-row hydrides change smoothly in going from left to right in the periodic table, rising to a maximum at group 2 and dropping to large negative values toward group 7 (53). This systematic change has been explained in terms of the change in the position of the equilibrium molecular geometry relative to the shielding surface (56). Figure 2 shows two examples.

Before any theoretical calculations were available, general trends in the derivatives of shielding surfaces at the equilibrium molecular geometry had been proposed by Jameson and coworkers (62–66) (see 66 for references) in their interpretation of the very large body of experimental isotope shift data and the temperature dependence of the chemical shifts in the zero-pressure limit of ^{19}F, ^{13}C, ^{15}N, ^{31}P, ^{77}Se, and other nuclei in small molecules. The ability of local origin methods to adequately describe the shielding even with modest basis sets has made it possible to theoretically investigate these conclusions and to find their limitations and conditions of applicability. A comprehensive survey of first and second derivatives of the shielding for molecules containing first-row atoms (67) confirmed the earlier predictions. Chesnut & Wright's (67) survey of shielding derivatives also offers new information about second derivatives: Most of the second derivatives are negative, but a fair number of those involving proton shieldings are positive.

Examination of the shielding dependence on bond length (derivatives were sufficiently large, -40 to -90 ppm/Å) in model fragments for glycine, alanine, and valine residues in proteins (36) permit an evaluation of the spread of bond length values for a particular residue reported in X-ray structures of proteins (68). The differences in bond lengths reported in X-ray structures are much

too large to be consistent with chemical shift inequivalencies observed in these residues in proteins.

Effects of Rovibrational Averaging

We discuss here those experimental observations that are due entirely to the dynamic averaging over the shielding surfaces. First is the observed temperature dependence of the chemical shift in the limit of zero density, where the number of collisions is sufficiently low that intermolecular interactions cannot account for the temperature dependence of the chemical shifts (69). The shielding of ^{19}F nuclei in molecules such as CF_4, SiF_4, BF_3, SF_6 (69), and F_2 (70) decreased as temperature increased, as in the examples shown in Figure 3. The observed

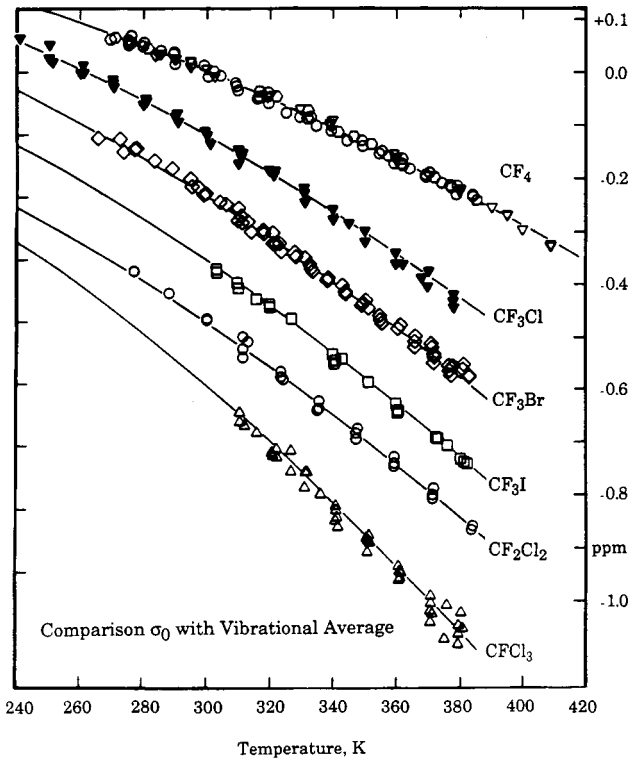

Figure 3 The temperature dependence of the ^{19}F shielding in several fluoromethanes in the isolated-molecule limit. The *y* axis is set to zero for the CF_4 molecule at 300 K; the other molecules have been arbitrarily displaced for clarity. The curvature in each case is a natural consequence of the nonlinear dependence on temperature of the dynamically averaged displacements of the C-F distance from its equilibrium value in an anharmonic system. [Reproduced from Reference 79a, with permission.]

temperature dependencies of the chemical shifts in isolated molecules were reasonably large; a nucleus such as ^{19}F with a large chemical shift range provides an easily measurable temperature coefficient, $-$ 0.001 to $-$ 0.034 ppm/degree, which parallels the paramagnetic shielding of ^{19}F in the molecule (64, 71). ^{13}C nuclei have considerably smaller shifts with temperature (72). Temperature coefficients have been measured for ^{11}B, ^{15}N, ^{13}C, ^{31}P, ^{77}Se, and ^{125}Te nuclei (59, 60, 71, 73–75). These observations were postulated to arise from the existence of a shielding surface that could be characterized by an expansion of the shielding in terms of nuclear displacement coordinates such as the internal coordinates or normal coordinates of the molecule (62, 76); the experimental value of the chemical shift was the thermal average of the shielding found by employing the thermal averages of the nuclear displacement coordinates. The general formulas have been derived in terms of these property derivatives and the derivatives of the potential energy surface (quadratic and higher force constants) (76–78). It was recognized fairly early that the anharmonic contributions to the mean bond displacement $\langle \Delta r \rangle^T$ (the so-called mechanical anharmonicity together with the centrifugal stretching associated with the rotational averaging for a nonrigid rotor) constitute the most important contributions (76, 79). There are, of course, contributions from the mean square displacement $\langle (\Delta r)^2 \rangle^T$ in the diatomic molecule, but these result from the counterpart of electrical anharmonicity, the second and higher derivatives of the shielding surface with respect to the bond stretch. We now know from the survey by Chesnut & Wright (67) of theoretical shielding derivatives in a large number of molecules that these terms are not necessarily small.

An equivalent approach, especially for larger excursions such as inversion, is to explicitly carry out the averaging over the vibrational wavefunctions and then to average over these according to the populations:

$$\langle \sigma \rangle^T = \frac{\sum_{\mathrm{vJK}} (2J+1) g_{\mathrm{Ns}} \langle \sigma \rangle_{\mathrm{vJK}} \exp(-E_{\mathrm{vJK}}/kT)}{\sum_{\mathrm{vJK}} (2J+1) g_{\mathrm{Ns}} \exp(-E_{\mathrm{vJK}}/kT)}.$$

The rovibrational averages $\langle \sigma \rangle_{\mathrm{vJK}}$ can be evaluated directly by integrating over the vibrational wavefunctions or in terms of the derivatives of the shielding surface with respect to nuclear displacements, as with any other molecular electronic property surface (77). The magnitudes of the rovibrational corrections relative to the shielding of the rigid equilibrium geometry are not small and should always be taken into consideration when making a comparison between the calculated shielding at the equilibrium molecular geometry and the experimental absolute shielding.

The mass dependence of the chemical shift was discovered even earlier than the temperature dependence (80); however, it was not until the recognition of the shielding surface that a single theoretical formalism could be established to

explain both phenomena (62, 63). It is in the context of the Born-Oppenheimer separation that the possibility of considering a molecular electronic property surface, such as the shielding surface, is achieved. In this context the shielding surface, being entirely an electronic property calculated for the various configurations of the nuclei, is the same for all isotopomers of the molecule. The observed mass dependence of the shielding is thus entirely a result of the differential dynamic averaging in a heavy isotopomer compared to the light one; on the average, the lighter isotopomer samples a larger region of the shielding surface than does the heavier isotopomer in its excursions away from the equilibrium molecular geometry (63). From the global shape of the shielding surfaces in Figure 2, we expect to find $\langle\sigma\rangle_{\text{heavy}} > \langle\sigma\rangle_{\text{light}}$ in the usual case (that is, like H_2^+). On the other hand, in those cases where the minimum on the potential energy surface happens to fall on the other side of the shielding surface where bond stretching lead to increased shielding, as for the Li or Na nucleus, the sign of the isotope shift is opposite to the usual; the larger excursions of the light molecule lead to a more shielded average than for the heavy molecule. Indeed, for isotopic substitution one to three bonds away, Li isotope shifts in organolithium compounds are found to be opposite to the usual sign (81, 82). The isotope shift is dominated by the bond stretching (60), even in the case of NH_3, where complete averaging over the inversion coordinate occurs at room temperature (59). It is not too surprising, then, to find that one-bond isotope shifts are fairly predictable in sign (66).

Although the shielding difference is best written out in terms of the two isotopomers, such as $[\sigma(^{15}\text{N}, ^{15}\text{NH}_3) - \sigma(^{15}\text{N}, ^{15}\text{ND}_3)]$, the commonly observed additivity in the isotope effects on shielding (80, 83, 84) allows the isotope shifts to be reported in terms of chemical shifts per isotopic substitution. The isotope shift is ubiquitous and literally thousands of examples are found in the literature (80, 85). The trends in isotope shifts has been explained theoretically (66, 86), including the additivity (87), the dependence on the fractional change in mass (88), and the observed linear dependence on $[1-(\mu/\mu')^{1/2}]$ or the $(m'-m)/m'$ factor for a series of isotopes of the same element (71, 88). These are dynamic factors that can be applied to isotope effects on molecular electronic properties in general. The isotope shifts in isolated molecules can now be said to be completely understood and can be calculated, in principle. For example, for the CO molecule, the observed temperature dependence of the ^{13}C shielding, the ^{13}C isotope shifts due to ^{17}O/^{16}O and ^{18}O/^{16}O substitution, and the ^{17}O shift due to ^{13}C/^{12}C substitution have all been calculated (89) and agree fairly well with experimental values (73, 90). The isotope shifts of ^{17}O in H_2O and D_2O, ^{15}N in $^{15}NH_3$ and $^{15}ND_3$, ^{31}P in PH_3 and PD_3, and ^{13}C in $^{13}CH_nD_{4-n}$, have all been calculated as a function of temperature by using the full shielding surfaces

for these nuclei (57, 59, 60, 91). A complete calculation for larger molecules may be limited by the lack of accurate potential energy surfaces or by the large number of nuclear displacement coordinates. Therefore, the knowledge gained from complete calculations using all the symmetry coordinates in these small molecules helps to gauge the limits of applicability of using a less complete picture, e.g using a dynamic average of a local displacement coordinate at the substitution site coupled with the shielding derivative with respect to that remote displacement. The observed two-bond and three-bond isotope shifts had been attributed to the nonnegligible derivative of the shielding with respect to the stretching of the remote bond at which the isotopic substitution has taken place (87, 92, 93). The usual fall-off of the magnitude of the isotope shift with the remoteness of the substitution had been explained in terms of these derivatives being generally smaller than those associated with the bond to the NMR nucleus (66). Theoretical shielding surfaces do confirm this (although there are many exceptions), as well as the fact that shielding derivatives with respect to a remote bond displacement are of either sign, although large values are usually negative (67).

The significant difference between σ_e and σ_0 (94) suggests that the quality of theoretical shielding calculations is best compared with absolute shielding measurements when the theoretical values have been computed for several geometries displaced from the equilibrium molecular configuration and the complete rovibrational averaging over the theoretical shielding surface is carried out to obtain a theoretical σ_0. The latter can then be compared with the σ_0 values obtained in the gas phase in the zero-pressure limit (94). On the other hand, chemical shifts measured in condensed phase also include intermolecular effects, which are considered below.

THE CONNECTION BETWEEN CHEMICAL SHIFTS AND ENVIRONMENT

The extreme sensitivity of the chemical shift to intermolecular effects makes it an excellent probe of environment. In most cases, hydrogen bonding and overlap and exchange with neighboring atoms give rise to medium shifts. Local magnetic fields and electric fields from neighbors sufficiently distant that no overlap or exchange needs to be taken into account nevertheless give rise to observable chemical shifts. For example, the magnetic field inside C_{60} due to the ring currents and the magnetizability of this molecule has been the subject of theoretical and experimental studies. ^{3}He encapsulated within C_{60} has a shielding of $+6.3 \pm 0.15$ ppm relative to the free He atom, whereas He in C_{70} has a shielding of $+28.8 \pm 0.2$ ppm (95). Theoretical calculations attempted

to reproduce this observed shielding (96–99). The geometry of the fullerene is the single most important quantity to get right; the closer the geometry is to the experimental geometry, the closer is the calculated shielding. The exact position of the He atom near the center of the cage hardly affects the results. That this shielding does not involve overlap and exchange between the fullerene and the rare gas atom is indicated by the fact that the calculated result for He and Ne are exactly the same for the same C_{60} geometry (96). Using MP2-TZP geometry for C_{60} and C_{70} leads to 8.7 and 24.0 ppm, respectively, in excellent agreement with experiment (98). When a series of fullerenes are considered, the endohedral He shielding increases in the same order as London-type ring-current calculations predict, i.e. $C_{60} < C_{84} < C_{82} < C_{78} < C_{76} < C_{70}$ (99). Current density methods permit the mapping of the diamagnetic and paramagnetic circulations at every point on and inside the fullerene and provide some explanation of its magnetizability and the endohedral shifts as well (97). Paramagnetic ring currents are associated with pentagons and interpreted as consequences of strong, local circulations about the formal double bonds of the C_{60} framework. C_{60} is concluded to be diamagnetic, but the interpretation of this diamagnetism as a sign of three-dimensional aromaticity is problematic.

The coefficients that determine the response of the nuclear shielding to an external uniform static electric field have been calculated for nuclei in various molecules by Raynes et al and Dykstra et al (in 35). An interesting result for ^{1}H in the binary hydrides (100) and in various types of C-H bonds (101) is that the linear electric field coefficients (shielding polarizability) are very similar in value (electric field along the C-H bond from C to H) with a mean of 70.0 ppm au. It appears that this may be transferable among (sp^3)C-H bonds. The mean quadratic coefficient (shielding hyperpolarizability) is 68.0 ppm au. These were finite field calculations at the SCF level. Although the linear electric field coefficients are relatively stable in going from SCF to correlated calculations, the quadratic coefficients specially for nuclei other than H are extremely sensitive to electron correlation (101a).

The effects of the very large numbers of distant atoms in a protein cannot be taken into account computationally by doing calculations of the entire protein. One approach to the shielding contributions due to distant parts of the protein has been suggested by Oldfield and coworkers(102–105): to replace the shielding contributions from distant residues by considering only the classical electric fields and field gradients generated by electrostatic models (AMBER point charges for example) at the nucleus in question coupled with the response of the nuclear shielding to such electric fields and field gradients. These ideas present two challenges. One is, how well does representing the solvent molecule by a

point charge model evoke the appropriate shielding response? Second, how well does the use of the product of the shielding polarizability with the electric field at the nucleus replace this response? The answer to the first question was obtained by comparing two ab initio shielding calculations: One is a supermolecule calculation for the solute molecule (^{19}F in fluorobenzene) in the presence of the solvent molecules (HF), and the other is for the solute molecule in the presence of the point charge models for the solvent molecules (102). The answer to the second question comes from comparing results obtained from full ab initio computations with those derived from the shielding polarizability approach: In order to reach agreement, terms up to the hypergradient of the field need to be considered (103). On the other hand, terms arising from the shielding hyperpolarizability can be neglected. In the real systems where there is motional averaging, the various electric field terms would average differently.

In the approach used by de Dios, Oldfield, and coworkers, the rest of the protein and/or the rest of the molecules in the crystal are modeled by partial point charges to account for the intermolecular effects, in addition to specific hydrogen-bonding effects modeled by including hydrogen-bonding partners in the molecular system used in the shielding calculations (104, 105). These effects have important consequences, primarily for the shielding of the carbonyl carbons in the peptides or proteins, less important for the C^{α} and C^{β}. For example, in a crystal of tyrosine (and threonine), the neighboring molecules in the zwitterionic lattice participate in three-dimensional networks of hydrogen bonds, with both the OH and CO_2^- groups being involved. All the carbon shielding tensors in the amino acids L-tyrosine and L-threonine have been determined experimentally. The ^{13}C shielding tensors in these crystals were calculated by de Dios et al using the GIAO method: one molecule with basis sets on all its atoms and the neighboring 32 additional molecules represented by point charges (104). When the shielding calculations were performed on the isolated molecule, the agreement between experimental tensor components and the calculated values were rather good except for two of the carboxylate shielding tensor elements in each amino acid. When the intermolecular effects are represented by the point charges as described above, the outlying carbonyl tensor components moved right onto the straight line, giving even better agreement with experiment. The directions of the principal axis systems are also given by the calculation, and they can be included in the comparison with experiment in the threonine single crystal study, by using the icosahedral representation suggested by Grant and coworkers (106). This shows excellent agreement with experiment (Figure 1). The three different components of the carboxylate shielding tensor exhibited different intermolecular effects: Intermolecular effects caused increased shielding for the least shielded components

(in the carboxylate plane, perpendicular to the C=O), the most shielded components (along the normal to the carboxylate plane) were hardly affected, and the intermediate components (in the carboxylate plane, along the C=O) showed decreased shielding in both amino acids (104). These are the same direction as the effects of hydrogen bonding on the shielding of carbonyl carbons in peptides and proteins shown by calculations in the model *N*-formylpenta-alaninamide in helical and β-turn structures (105). The most shielded component of the ^{13}C=O shielding tensor (perpendicular to the amide plane) is hardly affected by hydrogen bonding, the least shielded component (perpendicular to the C=O) goes toward increasing shielding with decreasing N $\cdots$ H $\cdots$ O distance, and the intermediate component is affected most of all, decreasing with decreasing N $\cdots$ H $\cdots$ O distance. The calculated helix-β-sheet difference is 4.9 ppm, with the helical site deshielded, in good agreement with the experimental observation that alanine helical sites are typically deshielded by about 4.6 ppm when compared with sheet or sheet-like residues. The results clearly show the importance of hydrogen bond interactions on carbonyl shielding both in the simple model compounds and in the penta-peptides; both the range and the sign of the experimental shifts are correctly predicted (105).

The Intermolecular Shielding Surface

Jameson suggested (107) that the shape of the intermolecular shielding function for two interacting rare gas atoms is similar to the shape of the H_2^+ intramolecular shielding surface; it has a minimum in the shielding at some internuclear separation close to the minimum of the potential energy surface. Previous theoretical calculations of intermolecular effects, suffering from gauge origin problems, exhibited a positive shielding in this vicinity, which would have given rise to a density dependence of opposite sign to that universally observed. The first theoretical indication of a minimum in the intermolecular shielding was obtained by Grayce & Harris (108), who calculated the prototypical intermolecular shielding function, the shielding surface of the triplet state of the H_2 molecule, by a truly gauge-invariant density functional method using an electron gas approximation. Because of the approximate nature of these calculations, the definitive shape of the intermolecular shielding function (such as in Figure 2) was not established until the LORG and second-order LORG (SOLO) calculations of the ^{39}Ar shielding in the interacting Ar-Ar system by Jameson & de Dios (109). Subsequently, the ^{39}Ar shielding in Ar-Ne, the Ne shielding in Ne-Ne and Ne-He (56), and the He shielding in the He-He system (35) were found to have the same shape. The latter exhibited a minimum only at the correlated level of calculation (MC-IGLO), whereas the correlation contributions to the ^{39}Ar shielding in the Ar-Ar system had been shown by SOLO calculations to be negligibly small. In all rare gas pairs the minimum in the

shielding surface occurs at a distance much shorter than r_0, the separation at which the potential energy of interaction goes to zero.

The shapes of the intermolecular shielding surfaces for rare gas pairs are very similar, and the nearly identical R dependence at separations around or larger than r_0 suggests that they may be conformal in the same sense that the law of corresponding states suggests that potential energy surfaces are conformal (109). The rare gas intermolecular shielding functions do scale according to the factors $\alpha_{\rm A} \cdot \langle a_0^3/r^3\rangle_{\rm A} \cdot \alpha_{\rm B} \cdot U_{\rm A}U_{\rm B}/(U_{\rm A} + U_B)$, for the shielding of A due to the presence of B, where α_A is the electric dipole polarizability of the rare gas atom in question and U_A is the first ionization potential of the atom. The characteristic $\langle a_0^3/r^3\rangle$ of the free atom in its ground state is the factor for the intrinsic shielding sensitivity (2, 3), and, to the extent that the shielding response is effected by the mutual distortion of the electron charge distribution of each atom in the presence of the other atom, the magnitude of the response could be related to the usual quantities that appear in the London model for dispersion energy. The scaled ^{39}Ar in Ar-Ar shielding function produced curves that were nearly superposable in the range of distances of interest with the ab initio shielding functions of other rare gas pairs (109). The ^{39}Ar shielding in Ar-Ar—scaled to the ^{129}Xe shielding in Xe-Ar, Xe-Kr, and Xe-Xe—gives second virial coefficients of the ^{129}Xe shielding in rare gas mixtures that are in excellent agreement with experiment in sign, magnitude, and temperature dependence (109).

The general shape of the shielding surface for ^{39}Ar interacting with Na^+ ion is similar to the ones for rare gas pairs (see Figure 2), but the R dependence at large separations is close to R^{-4} rather than to R^{-6} (56, 109). Similar results were found for ^{129}Xe interacting with H^+, Li^+, Na^+, and K^+ ions, whereas the ^{129}Xe shielding surfaces in the interaction with Cu^+ and Ag^+ ions show minimum shielding at separations greater than the r_{min} of the potential function (110). By a consideration of the shielding response to a point charge, electric dipole, quadrupole, etc, in the long-range limiting situation, it has been possible to understand the different distance dependence found for ^{39}Ar shielding in Ar $\cdots$ Na^+ ion compared to Ar $\cdots$ NaH (56). The latter has more nearly an R^{-6} dependence.

The problem of basis set superposition errors (BSSEs) is of great importance in calculating not only interaction energies but also molecular electronic properties. The problem of BSSE, an explanation of its origin, and the methods of circumventing it have been reviewed (111, 112). BSSEs in intermolecular shielding calculations are important because polarization functions and functions with diffuse exponents that are employed in shielding calculations are readily used by all monomers in the complex and yield BSSEs of the same order of magnitude as the interaction energy itself. The purpose of a good BSSE

correction scheme is to yield the true interaction energy (or molecular electronic property) corresponding to the quality of the basis set and the method of calculation. A standard approach to circumvent BSSE problems consists in the application of the counterpoise method by Boys & Bernardi (113). Each subsystem (monomer) is to be calculated in the complete basis of the supersystem.

In the calculation of the shielding surfaces of a rare gas atom in response to an aluminosilicate (zeolite) cage, the monomer (free Ar atom) shieldings to be used are calculated in the full supersystem (Ar plus zeolite fragment) basis. This is the so-called full counterpoise method. In these systems the BSSE in the ^{39}Ar shieldings is a function of position of the Ar with respect to the fragment and is of the order of a few parts per million (114). The ab initio value of the ^{39}Ar shielding at various positions relative to various 4-ring, 6-ring, 8-ring, and joined 4- and 6-ring neutral fragments of zeolites NaA, KA, and CaA were calculated. The zeolite fragments used were, respectively, $[Si_2Al_2O_4(OH)_8]^{2-}$ Na_2^+, $[Si_3Al_3O_6(OH)_{12}]^{3-}$ Na_3^+, and $[Si_4Al_4O_8(OH)_{16}]^{4-}$ Na_4^+ the analogous K^+ versions of these 4-, 6-, 8-rings, and the joined 4 + 6 ring $[Si_4Al_4O_9$ $(OH)_{14}]^{4-}$ Ca_2^{2+}, where the Si, Al, O atoms are all located at the coordinates taken from the single-crystal X-ray refinement of the dehydrated zeolites (114).

How does one represent the intermolecular shielding in a supersystem such as this? Intermolecular shielding is largely additive in polar and nonpolar systems. In the region where the internuclear distances are close to or larger than r_0 of the Ar_2 potential, the intermolecular shielding function for the central ^{39}Ar in the linear Ar_3 trimer and the Ar in the triangular trimer are nearly exactly superposable, with two times the intermolecular shielding function of Ar in the dimer (109). Therefore, except at close distances that are sampled only at extremely high temperatures or pressures, the intermolecular shielding of rare gas atoms is close to additive. The intermolecular chemical shifts from two up to five HF molecules at specific sites around the ^{19}F of a fluorobenzene molecule are reproduced by summing over the individual single HF solvation shifts (102). We assume then that the individual ab initio values for Ar in zeolite can be described by a pairwise additive sum,

$$\sigma\left(^{39}\text{Ar, Ar}\cdots\text{fragment} = \sum_i \sigma\,^{39}\text{Ar, Ar}\cdots\text{O}_\text{i}\right)$$
$$+ \sum_j \sigma\,(^{39}\text{Ar, Ar}\cdots\text{Na}_\text{j}),$$

where the isotropic shielding functions $\sigma(^{39}\text{Ar, Ar}\cdots\text{O}_\text{zeol})$, $\sigma(^{39}\text{Ar, Ar}\cdots\text{Na}_\text{zeol})$, $\sigma(^{39}\text{Ar, Ar}\cdots\text{K}_\text{zeol})$ and $\sigma(^{39}\text{Ar, Ar}\cdots\text{Ca}_\text{zeol})$ are taken to be of the form of a four-term linear combination in inverse powers of the Ar-O and Ar-M distances, based on the distance dependence of simple intermolecular shielding

functions (35, 56, 109). Since the Si and Al atoms are not included in fitting to the sums of atomic contributions to the ^{39}Ar shielding, the oxygen contribution $\sigma(^{39}\text{Ar, Ar} \cdots \text{O}_{\text{zeol}})$ is an effective shielding function that describes the effect of the entire framework (not including the cations). These functions are scaled to obtain the ^{129}Xe intermolecular shielding functions in zeolites.

The Second Virial Coefficient of the Chemical Shift

Observed intermolecular chemical shifts are averages over the intermolecular shielding surface. The shielding, just as any other molecular electronic property measured in the bulk, can be expressed in terms of an expansion in the density (115),

$$\sigma(T, \rho) = \sigma_0(T) + \sigma_1(T)\rho + \sigma_2(T)\rho^2 + \sigma_3(T)\rho^3 + \cdots,$$

where $\sigma_1(T)$ is the second virial coefficient of nuclear shielding. In the interpretation of the medium shifts in dilute gases, only two molecules need be considered in generating the supermolecule shielding surface. Given the theoretical shielding surfaces for rare gas pairs (56, 109), one then simply integrates over the intermolecular shielding surface using the intermolecular potential surface V(R) for a proper weighting of all possible configurations of the system. For example, the density coefficient of the ^{129}Xe chemical shift for Xe in Ar gas at infinite dilution is given by

$$\sigma_1(T) = 4\pi R^2 \int_0^\infty R^2 dR\{\sigma(R) - \sigma(\infty)\} \exp[-V(R)/kT].$$

The sign of $\sigma_1(T)$ is negative at all temperatures, that is, intermolecular effects are generally deshielding (79, 94). The calculated $\sigma_1(T)$ values for the ^{129}Xe nucleus in Xe-Ar, Xe-Kr, and Xe-Xe interactions in the gas phase are in good agreement with the experimental data: The signs are correct, the relative magnitudes are correct, and the temperature dependences are about right. With this, the density dependence of the chemical shift in the gas phase may be said to be understood. There are no other molecular electronic properties for which the second virial coefficient has been measured and interpreted theoretically (56, 109).

Fairly large $\sigma_1(T)$ values have been measured in the gas phase for ^{129}Xe, ^{31}P, and ^{19}F nuclei (94), smaller ones for ^{13}C (72). The observed σ_1 values are nearly uniformly negative, which implies that the portion of the intermolecular shielding function being averaged over is deshielding relative to the infinitely separated molecules. The striking examples of intermolecular shifts that have positive σ_1 values are the shifts of N nuclei in the types of nitrogen environments that involve low-lying $n - \pi^*$ excited states in the shielding, for example, HCN, MeCN, pyridine (116). To interpret these observations it is necessary

to calculate the whole shielding surface for at least the dimer and then do a proper averaging over the surface, in order to find $\sigma_1(T)$. HCN is known to form linear hydrogen-bonded complexes $(HCN)_n$ that leave the C-H bond intact upon exchange; a proper average would allow the size of the n-mers to vary. This type of averaging for several hydrogen-bonded systems is in progress in TC Farrar's laboratory. Below, we consider a system in which a proper average over all configurations of the n-mer is carried out at each temperature, leading to average chemical shifts that agree with experiment.

Gas-to-Liquid Shifts

An obvious intermolecular shift is the gas-to-liquid shift or the gas-to-solution shift. When exactly the same set of solvents are used and the chemical shifts of the solutes (in the limit of infinite dilution) can be compared, some interesting trends emerge. For example He, Ne, Kr, and Xe solution shifts have been measured in exactly the same set of organic solvents. The chemical shift ranges of Xe:Kr:Ne:He in the set of solvents are 250:140:15:0.78 ppm (117). The chemical shift ranges in these solvents are found to be proportional to the same factors, fundamental quantities that are properties of the rare gas atom in question, that have been used for scaling the shielding surfaces: $\langle a_0^3/r^3\rangle \alpha U$ (109). The ^{13}C chemical shift range in CH_4 dissolved in the same set of solvents is 9 ppm.

The gas-to-liquid shift $[\sigma_{liq} - \sigma_{vap}]$ at a given temperature is entirely an intermolecular shift and is a function of the change in $[\rho_{liq} - \rho_{vap}]$ with temperature. Many gas-to-liquid shifts have been measured for ^{19}F nuclei, and a selected few for other nuclei (39). It is interesting to compare the relative sensitivity of different nuclei to deshielding effects of the surrounding medium. The ^{17}O in H_2O and ^{77}Se in H_2Se gas-to-liquid shifts at 300 K are proportionately large (36 and 120 ppm, respectively), as may be expected, according to either the $\langle a_0^3/r^3\rangle$ for the atoms or the chemical shift ranges of O and Se nuclei, and the magnitudes of these shifts depend on temperature and the density of the liquid. In an attempt to reproduce and characterize gas-to-liquid shielding changes in water, ab initio GIAO calculations were carried out on central waters in clusters of ten waters derived from a molecular dynamics simulation. The calculated changes in the shieldings are in the proper range but recover only about half of the experimentally observed deshielding. The flexible water molecule employed in the simulation exhibits large geometry distortions (rovibrational effects) that contribute significantly to the deshielding calculated, especially for the ^{17}O nucleus (118).

In a constant pressure experiment the liquid density generally decreases with increasing temperature. The intermolecular chemical shift (apart from the contributions of the changes in the bulk susceptibility with changes in density) then becomes smaller with increasing temperature. For example, the increase

in shielding of the ^{129}Xe nucleus in XeF_2 molecule in solution with increasing temperature, with a fairly large temperature coefficient of 0.4718 ppm K^{-1} (119), is due to intermolecular effects. Since the expected temperature dependence for vibrational effects has the opposite sign, the observed temperature coefficient must be largely due to the decreasing effects of intermolecular deshielding with decreasing density of the solution. In contrast, in a constant volume experiment, the temperature coefficient of the ^{129}Xe shielding in the Xe_8 cluster trapped in an essentially rigid cage of zeolite NaA is -0.145 ppm K^{-1}, a decrease in shielding with increasing temperature due to Xe-Xe interactions (120). There is a recent review of intermolecular shielding surfaces, including hydrogen-bonded systems and pairs of rare gas atoms (39). A review of chemical shift measurements for rare gas atoms in organic liquids and liquid crystals summarizes the data in solutions (121).

Chemical Shifts of Adsorbed Species

Physisorption is a result of the intermolecular interactions between an adsorbate and the atoms of the host matrix. The sorbate-sorbate interactions affect the observed adsorption isotherms and other properties, including diffusion of the sorbate molecules through the host lattice. One particularly interesting example of this phenomenon is the intermolecular shift of the Xe nucleus due to the interactions with the atoms of a zeolite. The extremely high sensitivity of the ^{129}Xe NMR chemical shift to its environment has made the Xe atom a widely used probe of the structure of zeolites, polymers, graphite, coals, and other materials. In particular, the applications of Xe NMR spectroscopy to the investigation of the structure of zeolites has been the subject of a large number of publications, and those prior to 1991 have been reviewed (122–124). These shifts are large, on the order of tens and hundreds of parts per million. In the limit of zero Xe coverage, the ^{129}Xe NMR chemical shift has been observed to be sensitive to the structure of a zeolite, to its pore size, to its Al:Si ratio, and to the size and types of the cations that balance the charge in the aluminated zeolites. In the limit of zero Xe coverage, the only contributions to the chemical shift are the Xe- zeolite interactions. What is necessary for comparison with experiments is an appropriate average over all the possible locations of a single Xe atom with respect to the zeolite framework and cations in it, that is, an appropriate weighting of the various points on the ^{129}Xe shielding function corresponding to these positions. Furthermore, the effects of the sorbate-sorbate interactions on the chemical shifts are very large, with the ^{129}Xe chemical shift increasing as the average number of Xe atoms per unit cell increases.

The most interesting and challenging experimental data to be interpreted are the chemical shifts observed in the Xe, Xe_2, Xe_3, ... Xe_8 clusters trapped in the alpha cages of the zeolite NaA (125, 126a,b). Here, what is observed is

not an average chemical shift under fast exchange of the Xe with a very large number of cavities containing a variable number of Xe atoms, but rather the individual chemical shifts of trapped clusters of Xe atoms, Xe_1, Xe_2, Xe_3, ... Xe_8. The chemical shifts have been measured as a function of temperature and these pose a dynamical averaging challenge for the theory (125). The shielding of the ^{129}Xe in the Xe_n clusters changes according to n; the most deshielded nuclei are in the Xe_8 cluster, but the individual cluster shifts do not change with loading. The cluster shift is in the direction given by $\sigma_1(T)$ observed in the gas phase; however, the incremental change is not a fixed amount but increases slightly in going from 1 to 6. Furthermore, there is a big change in shielding in going from Xe_6 to Xe_7 and then again in going from Xe_7 to Xe_8. These are all consequences of the dynamic averaging over these various shielding surfaces. Given a potential function for the interaction of a single Xe atom with the zeolite framework and the Na^+ ions, assuming that the total potential energy is a sum over all the pairwise interactions at distances less than some cutoff distance, and given the interaction potential function for the Xe-Xe interactions, likewise taken to be pairwise additive, then the properly weighted large number of configurations (a million or so) can be summed in a grand canonical Monte Carlo (GCMC) scheme (120). At each of these configurations the shielding of every Xe nucleus is calculated. Ab initio shielding calculations for ^{39}Ar in the triangular and linear Ar_3 clusters have shown that as long as the Ar atoms do not get much closer than about $0.9r_0$, the isotropic shielding contributions can be obtained by additivity. We therefore construct the ^{129}Xe shielding surface as we go, summing up over all the atoms that are sufficiently close (less than 12 Å).

The approach is to treat the whole system (any number of Xe atoms per unit cell and atoms of the zeolite framework) as a supermolecule and to calculate the shielding function at each configuration by assuming that the intermolecular shielding is pairwise additive, that is, for a given ^{129}Xe nucleus the shielding is a sum of contributions from Xe-Xe as a function of distance to all the other Xe atoms, plus Xe-O as a function of distance to all the O atoms of the zeolite framework, plus Xe-Na^+ as a function of distance to all the Na^+ counterions. The Xe-Al and Xe-Si contributions are neglected; the Xe atom cannot get close to these atoms because of the O atoms bridging the Al and Si. The shielding surface, which changes with the numbers of neighbors as the numbers of sorbate atoms fluctuate in the grand canonical ensemble, is constructed on the fly by using the pair shielding functions σ(Xe-O_{zeol}), σ(Xe-Na_{zeol}), and σ(Xe-Xe) derived from ab initio calculations described above (109, 114). The isotropic ^{129}Xe shielding averaged over all the Xe atoms in a cluster is separately stored for each of the eight cluster types so that the average chemical shift for each Xe_n can be obtained. This is done at each temperature. The averages at various

temperatures can then be compared with the experimental chemical shifts at these temperatures. We show the results in Figure 4 (120). The calculated and experimental quantities being compared are in absolute terms, that is, the shieldings are relative to the free Xe atom in both calculation and experiment. The agreement of the GCMC average with experiment is excellent, especially considering that there are no adjustable parameters once the Xe-zeolite potential parameters are adopted. In this work, the Xe-Xe contributions to the ^{129}Xe chemical shift within the alpha cages are assumed to be the same as that in the dilute Xe gas, only the distribution of Xe-Xe distances in the Xe_n clusters in type A zeolites is different. That the increments between the Xe_n cluster shifts are well-reproduced, including their temperature dependence, might have been expected from the good agreement found in the gas-phase chemical shifts based on the same ab initio–derived Xe-Xe intermolecular chemical shift function

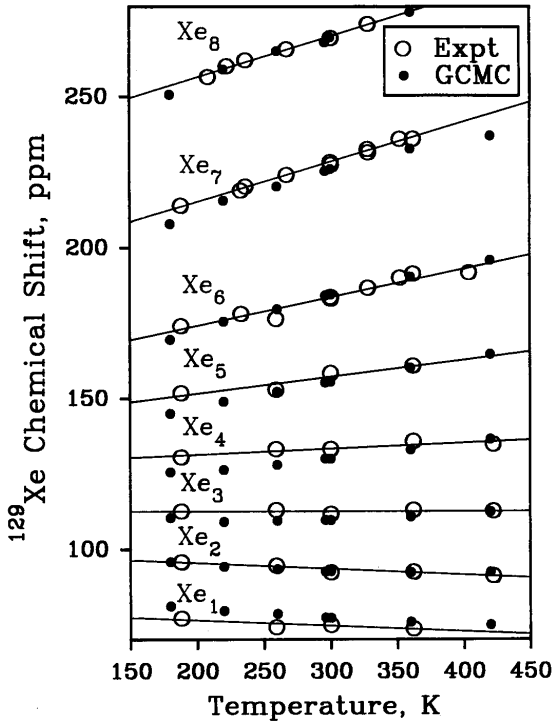

Figure 4 The temperature dependence of the average ^{129}Xe chemical shift in each of the Xe_n clusters trapped in the cages of zeolite NaA is reproduced by a GCMC average by using a sum of pairwise intermolecular shielding functions derived from ab initio calculations. [Reproduced from Reference 120 with permission.]

because these chemical shift increments are largely the result of the Xe-Xe interactions.

What about the changes in the intermolecular chemical shifts when the atoms of the zeolite cage are changed? The GCMC simulations permit examination of the separate contributions coming from the cations, the zeolite framework (effectively represented by the O atoms), and Xe-Xe contributions. The difference between the Xe-O and Xe-cation contributions in KA and NaA is interesting because the same $\sigma(\mathrm{Xe} \cdots \mathrm{O_{zeol}})$ and V(Xe-$\mathrm{O_{zeol}}$) functions were used in the GCMC simulations in both zeolites. The direct cation contribution to the chemical shift is larger for K than for Na in all cluster sizes, and this increases with cluster size. This is more pronounced in the KA cage as a result of the in-out arrangements of the K ions (127). The excluded volume effect due to the latter leads to smaller Xe-O contributions in KA and larger contributions from the Xe-Xe interactions, becoming more severe with increasing number of Xe atoms because of the more pronounced deshielding exhibited by the $\sigma(\mathrm{r}_{Xe-Xe})$ function at shorter distances. The net effect of the larger cation size on the Xe_n clusters is therefore to increase the chemical shift (found experimentally) and enhance the increments $[\delta(\mathrm{Xe}_n) - \delta(\mathrm{Xe}_{n-1})]$ (also observed experimentally) in KA compared to NaA. Although the calculated numbers can and do change upon changing the parameters of the V(Xe-K) potential, the trends are all preserved. The calculated differences between the chemical shift of Xe_n in KA and NaA are in semiquantitative agreement with experiment, and the GCMC simulations reproduce the trends for the temperature dependence of the ^{129}Xe chemical shifts of the Xe_n clusters in KA (127) just as well as they did for Xe_n in NaA (120). Under magic angle spinning, it has been possible to narrow the peaks corresponding to the Xe_n clusters in zeolite cages oriented in various directions relative to the magnetic field (128). Under these conditions, the Xe_n signals in the distinguishable cages that arise upon substitution of Ca^{2+} ions for Na^{+} ions in the same zeolite can be distinguished by their different intermolecular shifts: The progression of Xe_n signals associated with each cage type can be observed. [Incidentally, they have somewhat different distributions, as can be observed from the Xe_n intensities (128).] This is a dramatic illustration of the sensitivity of the ^{129}Xe shielding to the environment. Although the GCMC averaging has not been carried out for Xe_n in partially Ca^{2+} ion–exchanged NaA, the shielding function $\sigma(^{129}\mathrm{Xe}, \mathrm{Xe} \cdots \mathrm{Ca_{zeol}})$ can be used for this purpose (114), along with the shielding functions for the Xe, $\mathrm{O_{zeol}}$, and $\mathrm{Na_{zeol}}$ contributions that had already successfully reproduced the experiments in pure NaA.

In studies of competitive adsorption, the quantity that is usually measured is the overall composition of the adsorbed phase for a given composition of the

bulk phase in equilibrium with it. Chemical shifts can provide a more detailed description. In a mixture of Xe and Kr in NaA zeolite, Jameson et al (128) were able to observe the individual signals from Xe_nKr mixed clusters and the Xe_n clusters under magic angle spinning. The absolute ^{129}Xe chemical shifts of the Xe_nKr mixed clusters and the increments between Xe_nKr and the Xe_n are reproduced by GCMC averaging in various Xe-Kr mixtures in NaA zeolite, as shown in Table 1.

In the competitive adsorption of Xe and Ar in NaA zeolite, the Ar atoms are in fast exchange, so individual mixed clusters such as Xe_nAr_m cannot be observed. Here, the Xe_n peaks are observed just as in pure Xe in this zeolite, except that the individual chemical shifts are observed to be dependent on the loadings of Ar (primarily) and Xe (secondarily) (129). In Figure 5 we compare the experimental Xe_n cluster chemical shifts in 12 different samples of Xe-Ar mixtures in NaA with the average chemical shifts from the GCMC simulations with the same overall $\langle n \rangle_{Xe}$ and $\langle m \rangle_{Ar}$ as experiment. Here, the total intermolecular chemical shift measured relative to the isolated Xe atom, the ^{129}Xe chemical shift for Xe_n in an alpha cage with an average number of Ar atoms under fast exchange (which is directly calculated in the GCMC simulation), is plotted in comparison with the experimental values. We see that in an absolute measure, the calculated chemical shifts are in very good agreement with experiment. Furthermore, the differences in shielding, $[\langle \sigma(Xe_nAr_{ave}) \rangle - \langle \sigma(Xe_n) \rangle]$, may be compared directly with experiment, are a direct measure of the intermolecular effects of Ar, and are therefore a direct measure of the average number of Ar atoms in the cage with Xe_n. These calculated shielding differences are in quantitative agreement with experiment for samples with various Xe and Ar loading (129). The simulations also provide the average number of Ar atoms associated with each individual Xe_n. Once the average ^{129}Xe chemical shifts in

Table 1 ^{129}Xe chemical shifts of the mixed clusters Xe_nKr in the alpha cages of zeolite NaA (ppm)

Cluster	$\delta(Xe_nKr)$		$\delta(Xe_nKr) - \delta(Xe_n)$	
	OBSD[a,b]	GCMC[a,b]	OBSD	GCMC[b]
Xe_1Kr	84.7	85.8	9.9	8.5
Xe_2Kr	103.3	102.6	11.0	9.9
Xe_3Kr	124.5	121.5	12.8	11.9
Xe_4Kr	148.9	144.1	15.7	14.5
Xe_5Kr	174.7	172.0	16.3	17.2
Xe_6Kr	209.9	209.2	26.5	25.3

[a] Relative to an isolated Xe atom.
[b] From Reference 130.

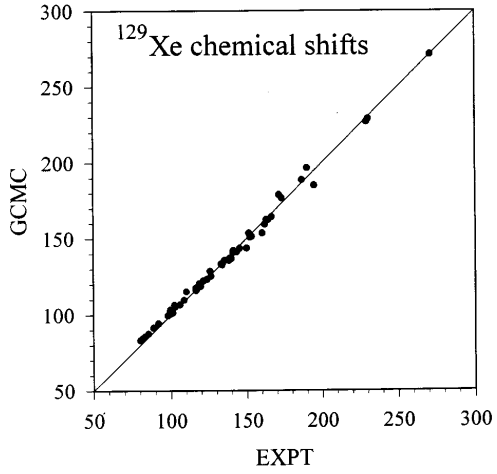

Figure 5 The ^{129}Xe chemical shifts (relative to the isolated Xe atom) of Xe_n in Ar under fast exchange in zeolite Na*A*, obtained from GCMC simulations compared with experimental values. [Reproduced from Reference 129 with permission.]

the Xe_nAr_m mixed cluster chemical shifts have been calculated for each *n* and *m* combination in the GCMC simulations, the Xe_n chemical shifts observed in any sample of Xe-Ar mixtures in zeolite NaA can be converted directly to the average number of Ar atoms in the same cage with *n* Xe atoms, while the fraction of cages containing exactly *n* Xe atoms is directly given by the relative intensity of the Xe_n peak. In other words, the ^{129}Xe chemical shifts provide the detailed distribution of the Xe-Ar mixture among the cavities of the zeolite. Other mixtures (Xe-CO, Xe-CO_2, Xe-CH_4, Xe-N_2,. . .) can be studied in this way.

CONCLUSIONS, CHALLENGES, AND FUTURE PROSPECTS

The NMR chemical shift serves as a paradigm for the effects of intramolecular dynamics and intermolecular interactions on molecular electronic properties. The combination of high-resolution measurements with the nuclear site specificity of the NMR chemical shift and the feasibility of ab initio quantum mechanical calculations has permitted the exploration of this electronic property surface and dynamic averaging on it. The ultra high resolution of NMR and the long relaxation times of nuclear spins permit the rovibrational effects on the property to be measured experimentally, providing detailed comparisons

between theory and experiment. The high quality of the experimental data imposes very stringent tests on descriptions of molecules provided by electronic structure calculations. Details of the property surface; its dependence on internuclear distances, bond angles, and torsion angles; and its response to electric fields and electric field gradients have been explored to a greater extent than any other molecular electronic property. The extreme sensitivity of the NMR chemical shielding tensor to molecular geometry provides very demanding tests of diffraction data (45, 68). The rovibrational averaging on the shielding surface leads to the observed temperature dependence in the gas at the zero-pressure limit and the mass dependence in the vast number of observed isotope shifts. Furthermore, the observed temperature dependence and mass dependence impose very stringent tests of anharmonic force fields for molecules. Averaging over the intermolecular collisions in a dilute gas leads to the observed temperature-dependent second virial coefficients of this property, again serving as an example for other molecular electronic properties. Only a proper dynamic averaging over the intermolecular shielding surface can account for the virial coefficients and their dependence on temperature and the nuclear site. Averaging the shielding function in a grand canonical ensemble leads to very good agreement with the observed temperature-dependent average chemical shifts of trapped Xe_n clusters inside the pores of zeolites, and provides the general approach to the interpretation of Xe chemical shifts as a probe of microporous solids and coadsorption.

The remaining challenges—in addition to relativistic and electron-correlated ab initio computations of shielding surfaces of molecules including heavy nuclei, such as those of transition and post-transition elements—are in the proper treatment of shielding of nuclei participating in extended covalent networks. These systems have so far been treated only at the empirical level; only small fragments of such networks have been treated quantum-mechanically, the $[SiO_4]^{-4}$ unit to represent silicates. Recently developed approaches to complex systems such as proteins provide new insight into the shielding-structure interdependence and may suggest possible approaches to ionic and covalent solids.

ACKNOWLEDGMENTS

The author thanks The National Science Foundation for support (Grants CHE-92-10790 and CHE95-28066).

Literature Cited

1. Ramsey NF. 1950. *Phys. Rev.* 78:699–703
2. Jameson CJ, Gutowsky HS. 1964. *J. Chem. Phys.* 40:1714–24
3. Jameson CJ, Mason J. 1987. In *Multinuclear Nuclear Magnetic Resonance,* ed. J Mason, pp. 51–88. London: Plenum
4. Lipscomb WN. 1966. *Adv. Magn. Reson.* 2:137–76
5. Lazzeretti P. 1995. *THEOCHEM-J. Mol. Struct.* 336:1–5
6. Lazzeretti P, Malagoli M, Zanasi R. 1991. *THEOCHEM-J. Mol. Struct.* 80:127–45

7a. Bishop DM, Cybulski SM. 1993. *Mol. Phys.* 80:199–208

7b. Bishop DM, Cybulski SM. 1993. *Mol. Phys.* 80:209–11

8. Dykstra CE, Liu SY, Malik DJ. 1989. *Adv. Chem. Phys.* 75:37–111
9. Geertsen J. 1989. *J. Chem. Phys.* 90:4892–94
10. Geertsen J. 1992. *Chem. Phys. Lett.* 188:326–31
11. Ditchfield R. 1974. *Mol. Phys.* 27:789–807
12. Wolinski K, Hinton JF, Pulay P. 1990. *J. Am. Chem. Soc.* 112:8251–60
13. Schindler M, Kutzelnigg W. 1982. *J. Chem. Phys.* 76:1919–33
14. Kutzelnigg W, Schindler M, Fleischer U. 1990. In *NMR Basic Principles and Progress,* 23:165–262. Berlin: Springer-Verlag
15. Hansen AE, Bouman TD. 1985. *J. Chem. Phys.* 82:5035–47
16. Facelli JC, Grant DM, Bouman TD, Hansen AE. 1990. *J. Comput. Chem.* 11:32–44
17. Keith TA, Bader RFW. 1992. *Chem. Phys. Lett.* 194:1–8
18. Ruud K, Helgaker T, Kobayashi R, Jörgensen P, Bak KL, Jensen HJA. 1994. *J. Chem. Phys.* 100:8178–85
19. van Wüllen C, Kutzelnigg W. 1993. *Chem. Phys. Lett.* 205:563–71
20. Gauss J. 1994. *Chem. Phys. Lett.* 229:198–203
21. Sauer SPA, Paidarova I, Oddershede J. 1994. *Mol. Phys.* 81:87–118
22. Sauer SPA, Paidarova I, Oddershede J. 1994. *Theor. Chim. Acta* 88:351–61
23. Gauss J, Stanton JF. 1995. *J. Chem. Phys.* 102:251–53
24. van Wüllen C. 1995. *J. Chem. Phys.* 102:2806–11
25. Vignale G, Rasolt M. 1987. *Phys. Rev. Lett.* 59:2360–63
26. Vignale G, Rasolt M. 1989. *Phys. Rev. B* 37:10685–96
27. Vignale G, Rasolt M, Geldart DJW. 1990. *Adv. Quantum Chem.* 21:235
28. Colwell SN, Handy NC. 1994. *Chem. Phys. Lett.* 217:271–78

29a. Malkin VG, Malkina OL, Salahub DR. 1993. *Chem. Phys. Lett.* 204:80–86

29b. Malkin VG, Malkina OL, Salahub DR. 1993. *Chem. Phys. Lett.* 204:87–95

30. Schreckenbach G, Ziegler T. 1995. *J. Phys. Chem.* 99:606–11
31. Grayce CJ, Harris RA. 1994. *Phys. Rev. A* 50:3089–95
32. Grayce CJ, Harris RA. 1995. *J. Phys. Chem.* 99:2724–26
33. Chesnut DB. 1994. *Annu. Rep. NMR Spectrosc.* 29:71–122
34. Jameson CJ. 1980–1996. *Nuclear Magnetic Resonance. Specialist Periodical Rep.* Cambridge: R. Soc. Chem.
35. Tossell JA, ed. 1993. *Nuclear Magnetic Shieldings and Molecular Structure. NATO ASI Ser. C,* Vol. 386. Dordrecht: Kluwer
36. de Dios AC, Pearson JG, Oldfield E. 1993. *J. Am. Chem. Soc.* 115:9768–73
37. de Dios AC, Oldfield E. 1994. *J. Am. Chem. Soc.* 116:5307–14
38. Le HB, Pearson JG, de Dios AC, Oldfield E. 1995. *J. Am. Chem. Soc.* 117:3800–7
39. de Dios AC, Jameson CJ. 1994. *Annu. Rep. NMR Spectrosc.* 29:1–69
40. Facelli JC, Orendt AM, Solum MS, Depke G, Grant DM, Michl J. 1986. *J. Am. Chem. Soc.* 108:4268–72
41. Solum MS, Facelli JC, Michl J, Grant DM. 1986. *J. Am. Chem. Soc.* 108:6464–70
42. Beeler AJ, Orendt AM, Grant DM, Cutts PW, Michl J, et al. 1984. *J. Am. Chem. Soc.* 106:7672–76
43. Carter CM, Alderman DW, Facelli JC, Grant DM. 1987. *J. Am. Chem. Soc.* 109:2639–44
44. Facelli JC, Grant DM, Michl J. 1987. *Acc. Chem. Res.* 20:152–58
45. Facelli JC, Grant DM. 1993. *Nature* 365:325–27
46. Duncan TM. 1990. *A Compilation of Chemical Shift Anisotropies.* Madison, WI: Farragut
47. Hegstrom RA. 1979. *Phys. Rev. A* 19:17–30
48. Stevens RM, Lipscomb WN. 1964. *J.*

Chem. Phys. 40:2238–47
49. Stevens RM, Lipscomb WN. 1964. *J. Chem. Phys.* 41:184–94
50. Stevens RM, Karplus M. 1968. *J. Chem. Phys.* 49:1094–100
51. Laws EA, Stevens RM, Lipscomb WN. 1971. *J. Chem. Phys.* 54:4269–78
52. Ditchfield R. 1981. *Chem. Phys.* 63:185–202
53. Chesnut DB. 1986. *Chem. Phys.* 110:415–20
54. Chesnut DB, Foley CK. 1986. *J. Chem. Phys.* 85:2814–20
55. Chesnut DB, Foley CK. 1986. *J. Chem. Phys.* 84:852–61
56. Jameson CJ, de Dios AC. 1993. *J. Chem. Phys.* 98:2208–17
57. Fowler PW, Riley G, Raynes WT. 1981. *Mol. Phys.* 42:1463–81
58. Lazzeretti P, Zanasi R, Sadlej AJ, Raynes WT. 1987. *Mol. Phys.* 62:605–16
59. Jameson CJ, de Dios AC, Jameson AK. 1991. *J. Chem. Phys.* 95:1069–79
60. Jameson CJ, de Dios AC, Jameson AK. 1991. *J. Chem. Phys.* 95:9042–53
61. Tossell JA, Lazzeretti P. 1988. *J. Magn. Reson.* 80:39–44
62. Jameson CJ. 1977. *J. Chem. Phys.* 66:4977–82
63. Jameson CJ. 1977. *J. Chem. Phys.* 66:4983–88
64. Jameson CJ. 1985. *Mol. Phys.* 54:73–79
65. Jameson CJ, Osten H-J. 1985. *J. Am. Chem. Soc.* 107:4158–61
66. Jameson CJ, Osten H-J. 1986. *Annu. Rep. NMR Spectrosc.* 17:1–78
67. Chesnut DB, Wright DW. 1991. *J. Comput. Chem.* 12:546–59
68. Laws DD, de Dios AC, Oldfield E. 1993. *J. Biomol. NMR* 3:607–12
69. Jameson CJ, Jameson AK, Cohen SM. 1977. *J. Chem. Phys.* 67:2771–74
70. Jameson AK, Schuett K, Jameson CJ, Cohen SM. 1977. *J. Chem. Phys.* 67:2821–24
71. Jameson CJ, Jameson AK, Oppusunggu D. 1986. *J. Chem. Phys.* 85:5480–92
72. Bennett B, Raynes WT. 1991. *Magn. Reson. Chem.* 29:946–54
73. Jameson CJ, Jameson AK, Wille S, Burrell PM. 1981. *J. Chem. Phys.* 74:853–56
74. Jameson CJ, Jameson AK, Parker H, Cohen SM, Lee CL. 1978. *J. Chem. Phys.* 68:2861–67
75. Jameson CJ, Jameson AK, Wille S. 1979. *J. Phys. Chem.* 83:3372–78
76. Jameson CJ. 1977. *J. Chem. Phys.* 67:2814–20
77. Jameson CJ. 1991. In *Theoretical Models of Chemical Bonding.* Part 3. *Molecular Spectroscopy, Electronic Structure and Intramolecular Interactions*, ed. ZB Maksic, pp. 457–519. Berlin: Springer-Verlag
78. Fowler PW. 1981. *Mol. Phys.* 43:591–600
79. Jameson CJ. 1980. *Bull. Magn. Reson.* 3:3–28
79a. Jameson CJ, Osten HJ. 1985. *Mol. Phys.* 55:383–95
80. Batiz-Hernandez H, Bernheim RA. 1967. *Prog. NMR Spectrosc.* 3:63–85
81. Eppers O, Gunther H. 1990. *Helv. Chim. Acta* 73:2071–82
82. Eppers O, Gunther H. 1992. *Helv. Chim. Acta* 75:2553–62
83. Wasylishen RE, Friedrich JO. 1984. *J. Chem. Phys.* 80:585–87
84. Wasylishen RE, Friedrich JO. 1987. *Can. J. Chem.* 65:2238–43
85. Hansen PE. 1988. *Prog. NMR Spectrosc.* 20:207–56
86. Jameson CJ. 1991. In *Isotopes in the Physical and Biomedical Sciences. Isotopic Applications in NMR Studies*, ed. E Buncel, JR Jones, 2:1–54. Amsterdam: Elsevier
87. Jameson CJ, Osten H-J. 1984. *J. Chem. Phys.* 81:4293–99
88. Jameson CJ, Osten H-J. 1984. *J. Chem. Phys.* 81:4300–5
89. Paidarova I, Komasa J, Oddershede J. 1991. *Mol. Phys.* 72:559–73
90. Wasylishen RE, Friedrich JO, Mooibroek S, Macdonald JB. 1985. *J. Chem. Phys.* 83:548–51
91. Raynes WT, Fowler PW, Lazzeretti P, Zanasi R, Grayson M. 1988. *Mol. Phys.* 64:143–62
92. Osten H-J, Jameson CJ, Craig N. 1985. *J. Chem. Phys.* 83:5434–41
93. Jameson CJ, Rehder D, Hoch M. 1987. *J. Am. Chem. Soc.* 109:2589–94
94. Jameson CJ. 1991. *Chem. Rev.* 91:1375–95
95. Saunders M, Jimenez-Vazquez HA, Cross RJ, Mroczkowski S, Freedberg DI, Anet FAL. 1994. *Nature* 367:256–58
96. Cioslowski J. 1994. *Chem. Phys. Lett.* 227:361–64
97. Zanasi R, Fowler PW. 1995. *Chem. Phys. Lett.* 238:270–80
98. Bühl M, Thiel W, Jiao HJ, Schleyer PvR, Saunders M, Anet FAL. 1994. *J. Am. Chem. Soc.* 116:6005–6
99. Bühl M, Thiel W. 1995. *Chem. Phys. Lett.* 233:585–89

100. Grayson M, Raynes WT. 1994. *Chem. Phys. Lett.* 218:270–75
101. Grayson M, Raynes WT. 1995. *Magn. Reson. Chem.* 33:138–43
101a. Jensen HJA, Private communications
102. de Dios AC, Oldfield E. 1993. *Chem. Phys. Lett.* 205:108–16
103. Augspurger JD, de Dios AC, Oldfield E, Dykstra CE. 1993. *Chem. Phys. Lett.* 213:211–16
104. de Dios AC, Laws DD, Oldfield E. 1994. *J. Am. Chem. Soc.* 116:7784–86
105. de Dios AC, Oldfield E. 1994. *J. Am. Chem. Soc*. 116:11485–88
106. Alderman DW, Sherwood MH, Grant DM. 1993. *J. Magn. Reson. A* 101:188–97
107. Jameson CJ. 1975. *J. Chem. Phys.* 63:5296–301
108. Grayce CJ, Harris RA. 1991. *Mol. Phys.* 72:523–35
109. Jameson CJ, de Dios AC. 1992. *J. Chem. Phys.* 97:417–34
110. Freitag A, van Wüllen C, Staemmler V. 1995. *Chem. Phys.* 192:267–80
111. van Lenthe JH, van Duijneveldt-van de Rijdt JGCM, van Duijneveldt FB. 1987. *Adv. Chem. Phys.* 69:521–66
112. Chalasinski G, Gutowski M. 1988. *Chem. Rev.* 88:943–62
113. Boys SF, Bernardi F. 1970. *Mol. Phys.* 19:553
114. Jameson CJ, Lim H-M. 1995. *J. Chem. Phys.* 103:3885–94
115. Buckingham AD, Pople JA. 1956. *Discuss. Faraday Soc.* 22:17–21
116. Jameson CJ, Jameson AK, Oppusunggu D, Wille S. 1982. *J. Chem. Phys.* 76:152–62
117. Seydoux R, Diehl P, Mazitov RK, Jokisaari J. 1993. *J. Magn. Reson. A* 101:78–83
118. Chesnut DB, Rusiloski BE. 1994. *THEOCHEM-J. Mol. Struct.* 120:19–30
119. Jokisaari JP, Ingman LP, Schrobilgen GJ, Sanders JCP. 1994. *Magn. Reson. Chem.* 32:242–47
120. Jameson CJ, Jameson AK, Baello BI, Lim HM. 1994. *J. Chem. Phys.* 100:5965–76
121. Jokisaari J. 1994. *Prog. Nucl. Magn. Reson. Spectrosc.* 26:1–26
122. Fraissard J, Ito T. 1988. *Zeolites* 8:350–61
123. Dybowski C, Bansal N, Duncan TM. 1991. *Annu. Rev. Phys. Chem.* 42:433–64
124. Barrie PJ, Klinowski J. 1992. *Prog. NMR Spectrosc.* 24:91–108
125. Jameson CJ, Jameson AK, Gerald RE II, de Dios AC. 1992. *J. Chem. Phys.* 96:1676–89
126a. Chmelka BF, Raftery D, McCormick AV, de Menorval LC, Levine RD, Pines A. 1991. *Phys. Rev. Lett.* 66:580–83
126b. Chmelka BF, Raftery D, McCormick AV, de Menorval LC, Levine RD, Pines A. 1991. *Phys. Rev. Lett.* 67:931
126. Jameson CJ, Jameson AK, Gerald RE II, Lim H-M. 1995. *J. Chem. Phys.* 103:8811–20
127. Jameson AK, Jameson CJ, de Dios AC, Oldfield E, Gerald RE II, Turner GL. 1995. *Solid State Nucl. Magn. Reson.* 4:1–12
128. Jameson CJ, Jameson AK, Lim H-M. 1996. *J. Chem. Phys.* 104:1709–28
129. Jameson CJ, Jameson AK, Lim H-M. 1996. To be published